SANDIA REPORT

SAND2004-0564
Unlimited Release
Printed February 2004

Theory and Experimental Study of Surfactant Effects on Epitaxial Growth of Compound Semiconductors

Ryan Wixom
University of Utah
Salt Lake City, Utah 84112

Prepared by Sandia National Laboratories
Albuquerque, New Mexico 87185 and Livermore, California 94550

Sandia is a multiprogram laboratory operated by Sandia Corporation,
a Lockheed Martin Company, for the United States Department of Energy's
National Nuclear Security Administration under Contract DE-AC04-94AL85000.

Issued by Sandia National Laboratories, operated for the United States Department of Energy by Sandia Corporation.

Available to DOE and DOE contractors from
U.S. Department of Energy
Office of Scientific and Technical Information
P.O. Box 62
Oak Ridge, TN 37831

Telephone: (865)576-8401
Facsimile: (865)576-5728
E-Mail: reports@adonis.osti.gov
Online ordering: http://www.osti.gov/bridge

Available to the public from
U.S. Department of Commerce
National Technical Information Service
5285 Port Royal Rd
Springfield, VA 22161

Telephone: (800)553-6847
Facsimile: (703)605-6900
E-Mail: orders@ntis.fedworld.gov
Online order: http://www.ntis.gov/help/ordermethods.asp?loc=7-4-0#online

SAND 2004-0564

Unlimited release
Printed February 2004

Theory and Experimental Study of Surfactant Effects on Epitaxial Growth of Compound Semiconductors

Ryan Wixom
University of Utah
Salt Lake City, Utah 84112

Sandia National Laboratories
P. O. Box 5800
Albuquerque, New Mexico

Abstract

The work discussed in this report was supported by a Campus Fellowship LDRD. The report contains three papers that were published by the fellowship recipient and these papers form the bulk of his dissertation. They are reproduced here to satisfy LDRD reporting requirements.

Table of Contents

Introduction

Organometallic vapor phase epitaxy (OMVPE) is used for fundamental research and commercial production of III-V electronic and optical devices. An understanding of the surface processes leads to improved control of epitaxial thin film properties and enables development of next-generation optoelectronic devices. A knowledge of the growth surface, obtained by experimental and computational means, has been helpful in exploring theories about morphological evolution, alloy composition, and ordering in a wide variety of materials systems. Surfactants are also proving to be an essential tool for engineering novel materials. The effects of surfactants such as Sb, Bi, and Te on GaP, InP, GaInP, and GaAs were studied by experiment and simulation. These surfactants were found to induce changes in surface structure, control ordering, and modify fundamental surface kinetics.

Surface photo-absorption (SPA) has previously shown that the surfactant Sb, present during epitaxial growth of GaInP, modifies the surface reconstruction, induces triple-period ordering, and results in bulk composition modulation. Due to the nature of the OMVPE environment, detailed *in-situ* study of atomic scale growth processes is not possible. Ab-*initio* calculations, making use of Density Functional Theory (DFT), were performed to identify Sb induced surface reconstructions on GaP and InP (001) surfaces. A method for calculating the surface energies of these reconstructions was developed and used to create surface phase diagrams for the surfactant covered alloys. Reconstructions predicted by these phase diagrams, with (4 X 3) and (2 X 3) periodicity, explain the triple-period ordering in GaInP grown with Sb surfactant.

The previously observed Sb induced composition modulation seen in GaInP indicates an increase in anisotropic adatom surface diffusion. Surfactant enhanced surface mass transport is certain to have other interesting consequences as well. To investigate this, the surfactant effects of Sb, Bi, and Te on the surface kinetics of GaAs were studied. Homoepitaxy of patterned GaAs (001) substrates was performed with increasing concentrations of surfactant. The morphological evolution of the singular surface and patterned features was studied by optical and atomic force microscopy (AFM). The lateral growth rates of patterned features were measured for the [110] and [-110] directions.

Both Sb and Bi enhanced the [-110] lateral growth rate as much as 300%, while having little effect on the orthogonal direction. A kinetic Monte-Carlo simulation was used to explore the range of possible surfactant mechanisms responsible for this dramatically anisotropic evolution of the patterned features. An increase in adatom hop frequency in the [-110] direction was identified as the most reasonable explanation and this hypothesis was corroborated by the simulation.

The surfactant Te also had interesting effects on the morphology of singular GaAs. While the lateral growth rates were not effected, the morphology of the singular surface and the profiles of the patterned features were significantly altered. The mounded singular surface, normally observed for GaAs (001 homoepitaxy, became atomically smooth with the addition of Te. Under high Te concentrations angular pits formed on the surface. Trenches, or regions of decreased vertical growth, also formed at the base of the patterned features. The side-wall angles of the trenches and pits were correlated and dependent on the Te concentration. These interesting changes in GaAs (001) morphology were interpreted as an increase in step velocity (sticking coefficient) and an increase in the Ehrlich-Schwoebel barrier. Kinetic simulations support this interpretation.

Increasingly, the fabrication of novel optoelectronic devices requires growth on patterned or non-ideal surfaces. The evolution of these surfaces is critical to resulting device performance. In addition to explaining interesting surfactant phenomena, this study has shown that surfactants will be an important tool for both researchers and device manufacturers.

Sb and Bi surfactant effects on homo-epitaxy of GaAs on (001) patterned substrates

R.R. Wixom, L.W. Rieth, G.B. Stringfellow

Department of Materials Science and Engineering, University of Utah, Salt Lake City, Utah 84112

Abstract

Anisotropic lateral growth during GaAs (001) epitaxy can have dramatic effects on the evolution of patterned features and surface morphology. Many new opto-electronic devices require growth on patterned or non-ideal surfaces. Controlling lateral growth will be essential for the production of these devices. In this study, GaAs epilayers were grown by organometallic vapor phase epitaxy on patterned GaAs (001) wafers. During these growth experiments, trimethylantimony and trimethylbismuth were used as surfactant precursors to investigate the effects of Sb and Bi on GaAs lateral growth rates. Both surfactants were found to enhance the [110] lateral growth rate by nearly 300 %, while having a negligible effect on the lateral growth rate in the orthogonal direction. Kinetic simulations assisted in determining a plausible surfactant mechanism: The enhanced [110] lateral growth rate is due to an increase in the frequency of [110] diffusion events (decreased hop barrier).

1 Introduction

Organometallic Vapor Phase Epitaxy (OMVPE) is used for research and commercial production of III-V electronic and optical devices. Understanding OMVPE growth phenomena is a key to the high-yield fabrication of state-of-the-art electronic and photonic devices. Epitaxy, performed under typical conditions, on the GaAs (001) surface proceeds by the incorporation of adatoms at [$\bar{1}$10] and [110] steps. For most growth conditions, these steps propagate at very different rates, which are dependent on temperature and the group V partial pressure. As a result, lateral growth anisotropy can have dramatic effects on the evolution of surface morphology. Islands, mounds, and patterned features will evolve anisotropically, elongating in the direction of faster lateral growth. For OMVPE this is the [110] direction.

Many novel opto-electronic devices and low-dimensional structures require epitaxy on patterned or non-ideal surfaces. The anisotropic evolution of these

Preprint submitted to Elsevier Science *11 November 2003*

features must be accounted for and could complicate the task of device fabrication. Fortunately, this phenomenon can be controlled and might even be used as a technique for novel device fabrication. In addition to the technological applications, information about fundamental crystal growth physics can be extracted from experiments involving lateral growth on patterned substrates.

The early work of Asai [1] showed that it is possible to modify GaAs(001) lateral growth rates by controlling the growth temperature or the AsH_3 overpressure. The effects of substrate mis-orientation have also been studied [2,3]. The presence of Cl on the surface, from the addition of CCl_4 to the vapor, has also been shown to modify lateral growth rates [4]. This is an attractive method of controlling lateral growth rates, but the use of CCl_4 might have limited application due to the high carbon doping introduced and the modification of total growth rate and/or alloy composition caused by halides [5]. Environmental concerns also limit the desirability of using this particular precursor. However, these results suggest that an ideal method for modifying the lateral growth rate may be through the addition of small concentrations of surfactants. It is expected that surfactants isoelectronic with one of the host elements will be the most desirable, due to the absence of doping effects. This method is easy to implement, allows for otherwise constant growth parameters, and would not affect carrier concentrations within the layer.

Use of surfactants has, in recent years, emerged as a simple yet powerful tool for engineering epitaxial surface processes. Surfactants are active surface species having a negligible solubility in the bulk. The large group V elements, such as Sb and Bi, are excellent isoelectronic surfactants easily introduced to the growing surface via common organometallic precursors. Sb and Bi containing organometallics are already widely used in commercial and research reactors for doping (in group IV semiconductors) and alloying (in III/V semicondutors). The surfactant effects of Sb have been studied on GaInP [6–12], GaN [13–15], (GaIn)(NAsSb) [16], InGaAs [17], and GaAs [18,19]. Bi surfactant effects have been studied on GaInP [7,9], GaAs [19], InGaAs [20,17], InGaNAs [21], Si [22], and during the fabrication of InAs quantum dots [23]. These two surfactants have been reported to modify ordering, composition modulation, dopant incorporation, adatom diffusion, and surface structure.

This paper describes the use of Sb and Bi as surfactants to control GaAs (001) lateral growth. GaAs epilayers were grown by OMVPE on patterned GaAs(001) wafers with increasing amounts of trimethylantimony (TMSb) or trimethylbismuth (TMBi) in the vapor. The resulting surface morphology and lateral growth rates were characterized by atomic force microscopy (AFM) and Nomarski optical microscopy.

The OMVPE environment does not easily lend itself to *in-situ* study of atomistic surface processes. To enhance our understanding of relevant surface pro-

cesses we used a simple kinetic simulation to correlated atomistic parameters and observed experimental results.

2 Experimental Procedures

Standard photo-lithography was used to pattern groups of shapes onto a singular GaAs (001) wafer. Each group contained a cross (having four $20 \times 10\mu$m arms), square ($20 \times 20\mu$m), a diamond (20μm diagonal), and a circle (10μm radius), with 50 μm between each shape and 500 μm separating each repeated group. A solution of NH_4OH:H_2O_2:H_2O (2:1:12) was used to etch the wafers at a rate of $\sim$ 15 nm/s for 12 s, creating 180 nm tall features from the patterned shapes. The photo resist was removed and the substrates were degreased with trichloroethylene, acetone, and methanol before being rinsed with deionized water and blown dry with N_2. The GaAs epilayers were grown by OMVPE in a horizontal flow, infrared heated, atmospheric pressure reactor. The precursors TMGa and AsH_3 were diluted in purified (Aeronex Gatekeeper) H_2 carrier gas with a total flow of 4000 sccm. A growth temperature of 620 °C, input V/III ratio of 30, and TMGa partial pressure of 6.4×10^{-2} Torr resulted in a vertical growth rate of $\sim$ 2 μm/hour.

For studying the surfactant effects of Sb (Bi), the TMSb/V (TMBi/V) ratio was varied from 0 to 0.0055 (0.006). Also, several GaAs epilayers were grown without surfactants for increasing times, from 5 to 40 min. This time dependent series of experiments was repeated with a constant TMSb/V ratio of 0.005.

The epilayers as well as the initial patterned wafer were characterized using Nomarski differential interference contrast optical microscopy and atomic force microscopy (AFM). AFM measurements were made with a Digital Instruments Dimension 3000 in Tapping Mode. AFM cross-section data of the patterned features was used to measure lateral growth rates in the $[\bar{1}10]$ and [110] directions, measure RMS roughness, and analyze changes in the morphology of the patterned mesas.

3 Kinetic Simulation

To compliment our *ex-situ* surface analysis, we have used a simple kinetic simulation to investigate which surface processes are modified by the addition of surfactants. This simulation assumes a two dimensional simple cubic lattice, where vacancies, overhangs, and desorption are not allowed. A randomly distributed flux of adatoms is adsorbed onto the surface at the start of each time

step. Atoms on the surface diffuse by randomly hopping, at a specified hop frequency, to adjacent surface sites. When diffusing atoms encounter a step, their incorporation, rejection, or continued progress is determined by up and down sticking coefficients and an Ehrlich-Schwoebel (E-S) barrier [24,25]. At the completion of each time step, the adatom concentration for each terrace is calculated. If the concentration exceeds a predetermined fraction for any terrace, a nucleation event occurs at that location. An input file specifies the initial profile, if any, and the growth parameters: growth rate, hop frequency, up and down sticking coefficients, E-S barrier, and nucleation criteria.

Since the diffusion length is dependent on hop frequency, sticking coefficients, and the E-S barrier, it varies with the local surface topology. The surface diffusion coefficient is often assumed to be described by the Arrhenius equation, $D=D_o\exp(-E_a/k_bT)$. Where E_a is the magnitude of the diffusion hop barrier, and D_o is a prefactor containing lattice and attempt frequency information. Even when considering a one dimensional simulation, it is tempting to make the necessary assumptions about the value of D_o to calculate a diffusion coefficient. However, even if the assumed values for D_o and E_a are accurate, this equation neglects local topology. Furthermore, reliable experimental data, for making comparisons, is not available. Hop frequency is a more physically meaningful parameter than diffusion coefficient because processes at step edges and the diffusion of adatoms across an atomically flat terrace are decoupled. In this simulation, adatom diffusion is characterized as a hop frequency, and the results will be discussed in terms of this frequency of diffusion events, rather than the diffusion coefficient.

The E-S barrier is essentially an increase in the hop barrier energy at the upper side of a step edge [24,25]. In the simulation this is implemented as a probability, but is easily converted to physically meaningful units, eV, which is how we have reported the values for this parameter in this work. Sticking coefficients are empirical and are reported in terms of the probability of an adatom incorporating as it diffuses across a step.

The effects of hop frequency, sticking coefficients, and E-S barrier on the surface profile resulting from simulated growth were investigated by systematically modifying the simulation input parameters and comparing the results to our experimental data. The spatial scale of the simulation was varied from 2 μm to 20 μm. However, as in the experiments, small features evolved similarly to large features and larger scale simulations were not always necessary. The temporal scale of the simulation was directly correlated to actual growth times at similar growth rates.

4 Experimental Results

The optical micrographs in fig. 1 show $\sim$ 180 nm tall cross-shaped mesas for a patterned substrate (A), after growth of a GaAs epilayer (B), and after growth of epilayers with TMSb (C) and TMBi (D) added to the vapor. Except for the use of surfactants, the nutrient precursor partial pressures, growth time, and all other growth parameters were held constant. These micrographs qualitatively illustrate the dramatic effect that Sb and Bi have on the anisotropy of the lateral growth rates. The main features are that both surfactants markedly increase the [110] growth rate, leaving the [$\bar{1}$10] growth rate either unchanged or even slightly decreased. The cross sectional shape of the patterned features is also seen to change noticeably. In addition, the surface apparently roughens, especially for the addition of Bi.

For a more quantitative description of the results, we have used AFM scans of originally square mesas to create the [$\bar{1}$10] and [110] surface profiles seen in figs. 2, 3, 4, and 5. These profiles are rich with information about how surfactants have modified the fundamental growth processes occurring at the surface. The data in these figures have been artificially shifted so the left sidewalls of all the mesas are inline. In each figure, the bottom profile is that of a patterned mesa prior to growth, the profiles above it are from samples grown with increasing surfactant concentrations.

The most remarkable feature observed from fig. 2 is the rapid monotonic increase in the [110] lateral growth rate caused by the presence of Sb. However, as shown in fig. 3, the lateral growth rate in the orthogonal direction is virtually unaffected. The lateral growth rates, as a function of Sb and Bi concentration, were measured and are shown in fig. 6.

Like Sb, Bi has a large effect on the [110] lateral growth rate, enhancing the anisotropy of the surface. However, notice that in this case the increase is not monotonic. For higher partial pressures of TMBi, the trend reverses and the [110] lateral growth rate begins to decrease. There is also a notable change in the mesa shape and surface morphology at these high Bi concentrations, that can be seen in both the [$\bar{1}$10] and [110] profiles.

A striking feature of the [$\bar{1}$10] profiles for both Sb and Bi samples is the "trenches", regions of depressed vertical growth rate formed adjacent to the mesa sidewalls. The appearance of these features coincides with the change in morphology of the terrace regions. A higher frequency and amplitude of the surface undulations is observed along this direction. Generally, the [110] profiles are smoother. The RMS roughness, obtained from the AFM data, increased from 3-5 nm for samples grown without surfactant, to 8 nm for the highest concentrations of TMSb and TMBi.

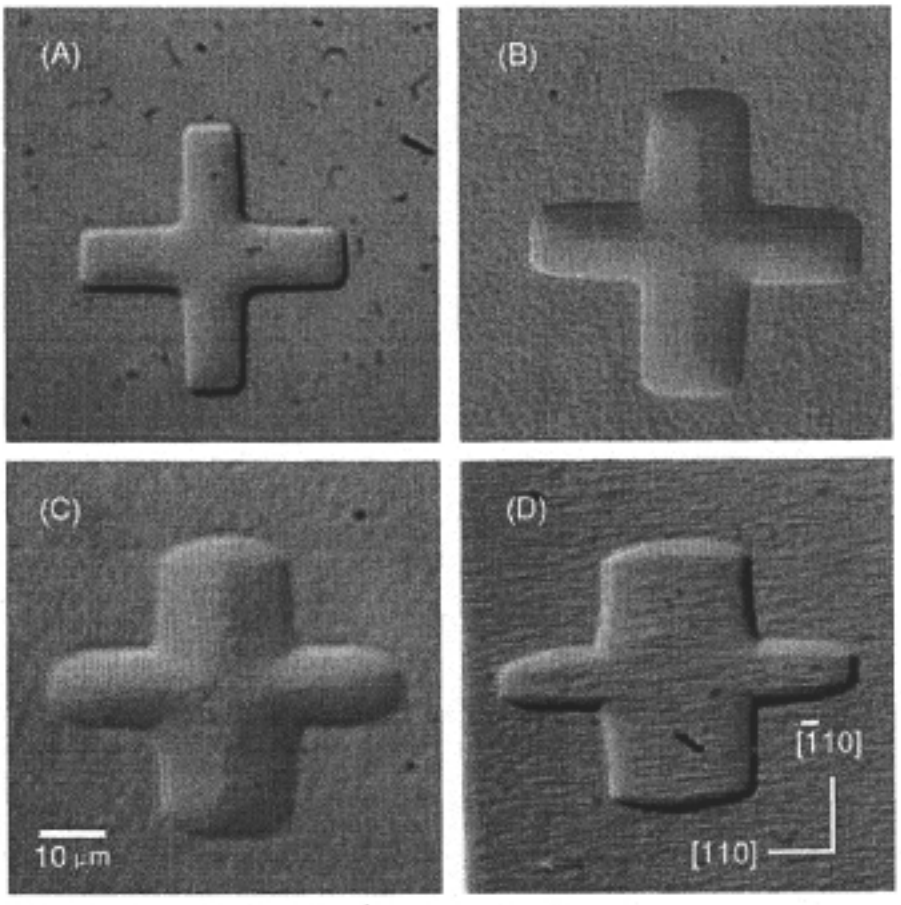

Fig. 1. Nomarski optical micrographs. (A) Patterned GaAs (001) wafer. (B) After 10 min. of growth with no surfactant. (C) 10 min. of growth with TMSb/V = 0.0055. (D) 10 min. of growth with TMBi/V 0.002.

The lateral spread of the mesa features is quantified as a lateral growth rate, with units of μm/hour. In order to validate this terminology, a temporal study was completed with and without TMSb in the vapor. In both instances, the mesa widths were measured from AFM scans and the data clearly shows a linear increase in lateral dimension with time. This justifies the presentation of the data as a growth rate.

5 Theory and Discussion

Adatoms preferentially incorporate at steps and kink sites rather than on a terrace due to a higher binding energy at sites where adatoms can make

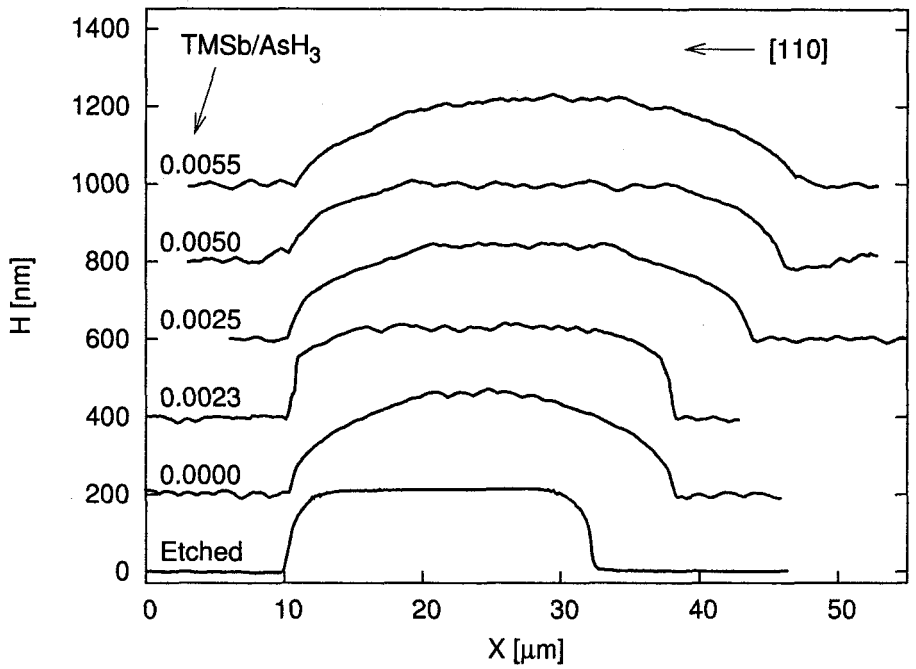

Fig. 2. AFM profiles of the [110] direction. All samples were grown for 10 min. with constant growth parameters except for increasing vapor phase TMSb/V ratio.

more bonds to the surface. However, the sticking coefficient at a step is not unity and the propagation of surface steps depends both on the arrival of adatoms and the sticking coefficient at the step. If the distance between steps is significant compared to the diffusion length, adatoms can build up on the terrace until nucleation of an island occurs. If either the surface diffusion coefficient or sticking probability is low, terraces will become super-saturated with adatoms and vertical growth will proceed by nucleation of new islands rather than lateral propagation of existing steps. Typically lateral spread of mesa sidewalls occurs at a much greater rate than vertical growth because propagation of existing steps is favored over nucleation.

GaAs is known to exhibit lateral growth anisotropy, for which there are two possible explanations. The first, is to attribute the anisotropy to differences in sticking coefficients at $[\bar{1}10]$ and [110] steps, postulating that steps on the [110] mesa sidewalls ($[\bar{1}10]$ steps) grow at an increased rate because of the structural differences between the two types of steps [1]. The second possibility is that, due to the asymmetry of the surface reconstruction, $[\bar{1}10]$ and [110] diffusion coefficients are not equal [2,3]. It is reasonable to expect that the phenomenon is, in fact, due to a combination of both effects, since either can limit the lateral propagation of surface steps.

From a simple qualitative examination of the mesa profiles, with both Sb and

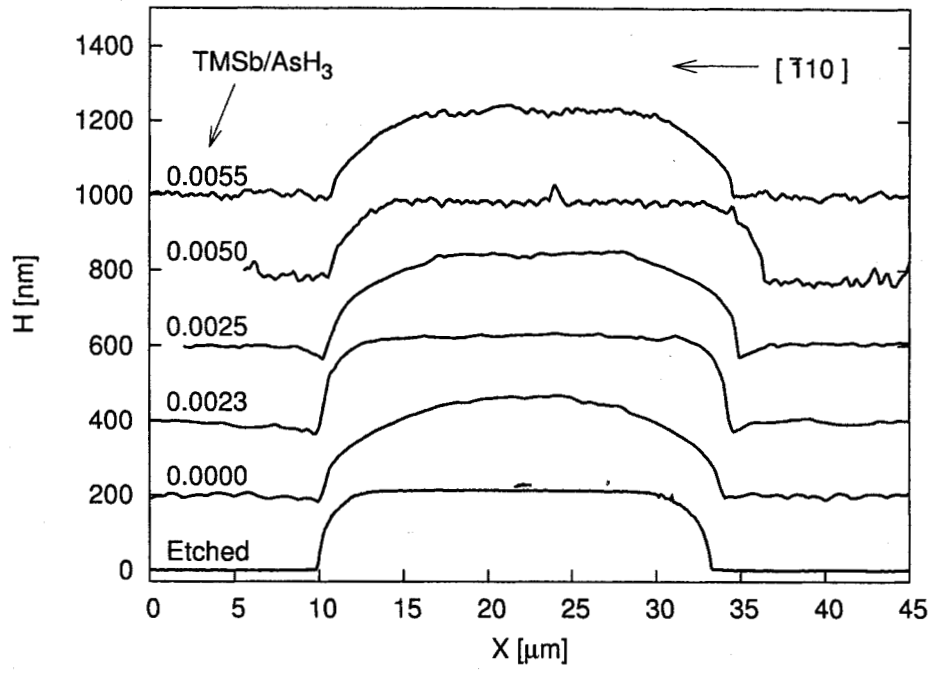

Fig. 3. AFM profiles of the [$\bar{1}$10] direction. All samples were grown for 10 min. with constant growth parameters except for increasing vapor phase TMSb/V ratio.

Bi, it appears that the [110] profiles are smooth and rounded as compared to the more jagged morphology exhibited for the [$\bar{1}$10] profiles. Also, trenches appear at the edges of mesa sidewalls in the [$\bar{1}$10] profiles. These observations are consistent with anisotropic surface diffusion. It is intuitively obvious that the frequency and amplitude of surface undulations are indicative of the amount of diffusion on the surface, considering the case of infinite diffusion length where growth of the crystal would proceed via the propagation of one step and nucleation of new islands would not occur. Conversely, if diffusion of adatoms were eliminated, the surface would statistically roughen as the thickness of the layer increased.

Results from kinetic simulations elucidate this discussion. The hop frequency was determined to be the key kinetic parameter affected by addition of the surfactant. Variations of the other growth parameters considered reproduced neither the large increase in lateral growth rate nor the shapes of the mesa profiles, which differed distinctly from those observed experimentally. Increasing the sticking coefficients resulted in mesa side walls having a concave profile. Decreasing the sticking coefficients resulted in a high rate of nucleation, statistical roughening of the surface, and no appreciable change in the shape of the patterned mesa. Increasing the E-S barrier resulted in a mounded morphology with increasing vertical rather than lateral growth. However, increasing the hop frequency over the range $10^4 - 10^6$ s^{-1} produced a large change in

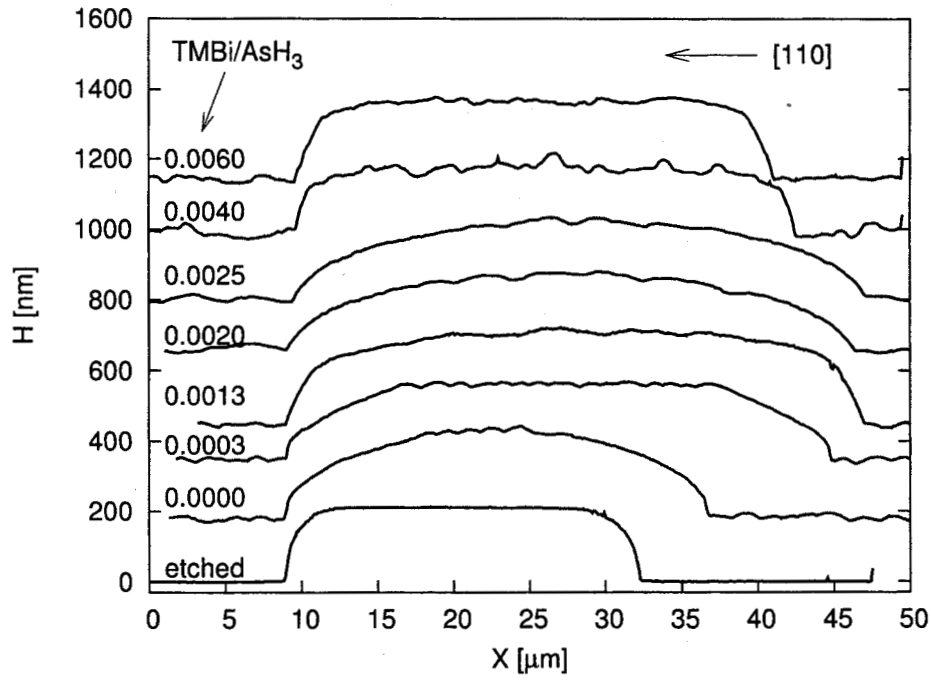

Fig. 4. AFM profiles of the [110] direction. All samples were grown for 10 min. with constant growth parameters except for increasing vapor phase TMBi/V ratio.

the lateral growth rate and mesa profiles closely resembling those observed experimentally. Thus, we are able to confidently interpret the experimentally observed surfactant induced increase in lateral growth as being primarily due to enhanced [110] diffusion.

The data in fig. 7 illustrate how the simulated lateral growth rate depends on the hop frequency. The hop frequencies used in the simulation are indicated in the figure and the other kinetic parameters were set at reasonable values: growth rate = 2 μm/hour, E-S barrier = 0.0 eV, up sticking coefficient = 0.003, and down sticking coefficient = 0.005. The lateral growth rates were calculated from simulated profiles in a manner similar to the experimentally measured lateral growth rates. The simulated and experimental data cover the same range and indicate a correlation between the presence of surfactants and the frequency of diffusion events on the terraces.

The conclusion that Sb increases adatom hop frequency is supported by the results of a previous study, where Sb was found to induce a compositional modulation in GaInP in the [110] direction [7]. This effect was attributed to an increased [110] surface diffusion coefficient. Sb was reported to substitute for group V atoms in the surface reconstruction without changing the surface structure [6,7,11,12]. The same result was reported for Sb on the surface of InGaAs [17]; We assume that Sb behaves similarly on the GaAs surface as

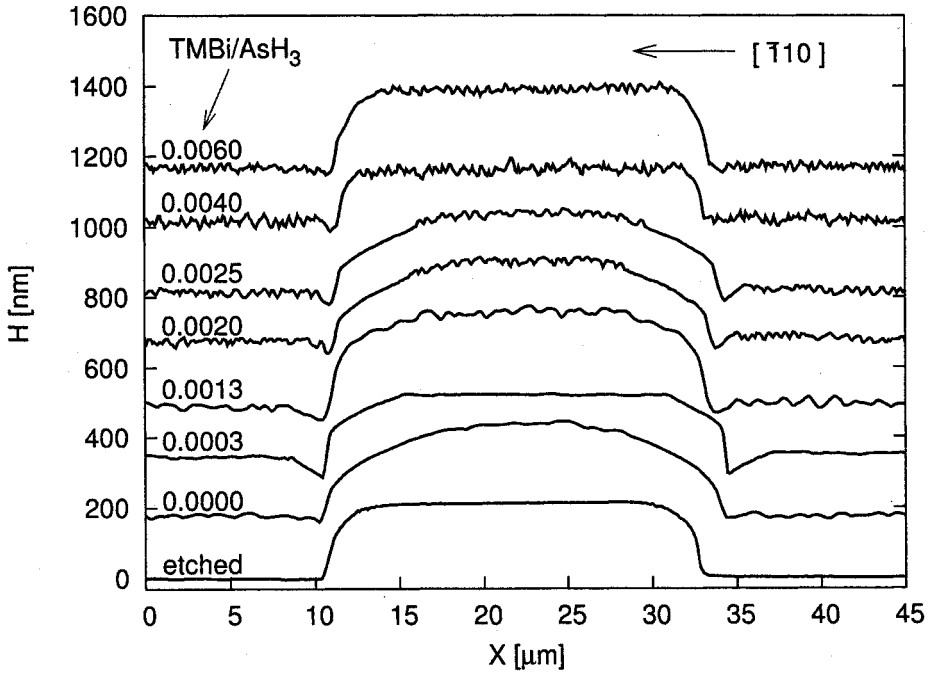

Fig. 5. AFM profiles of the [1̄10] direction. All samples were grown for 10 min. with constant growth parameters except for increasing vapor phase TMBi/V ratio.

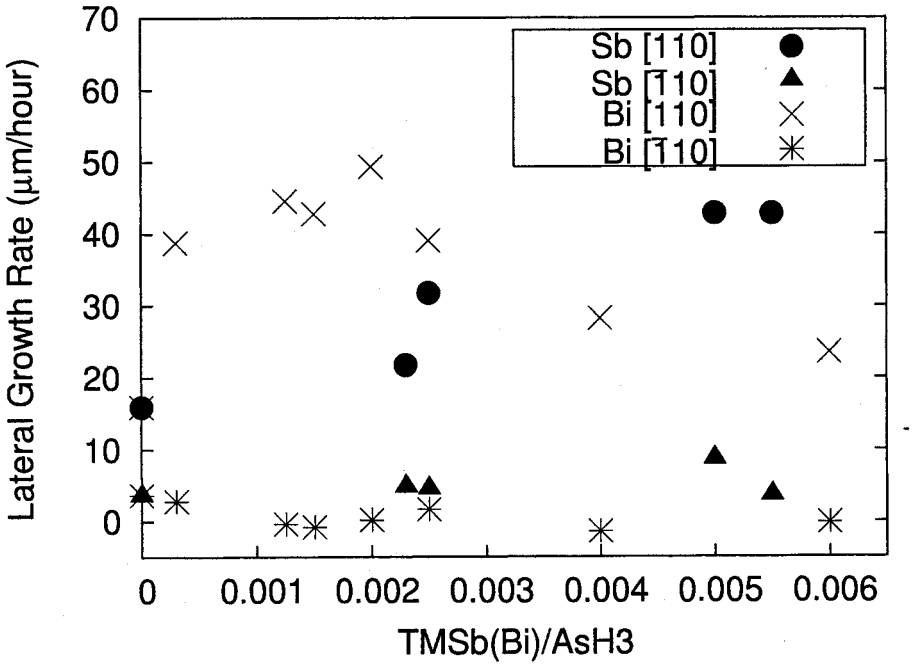

Fig. 6. Measured [110] and [1̄10] lateral growth rates for samples grown with surfactant Sb or Bi.

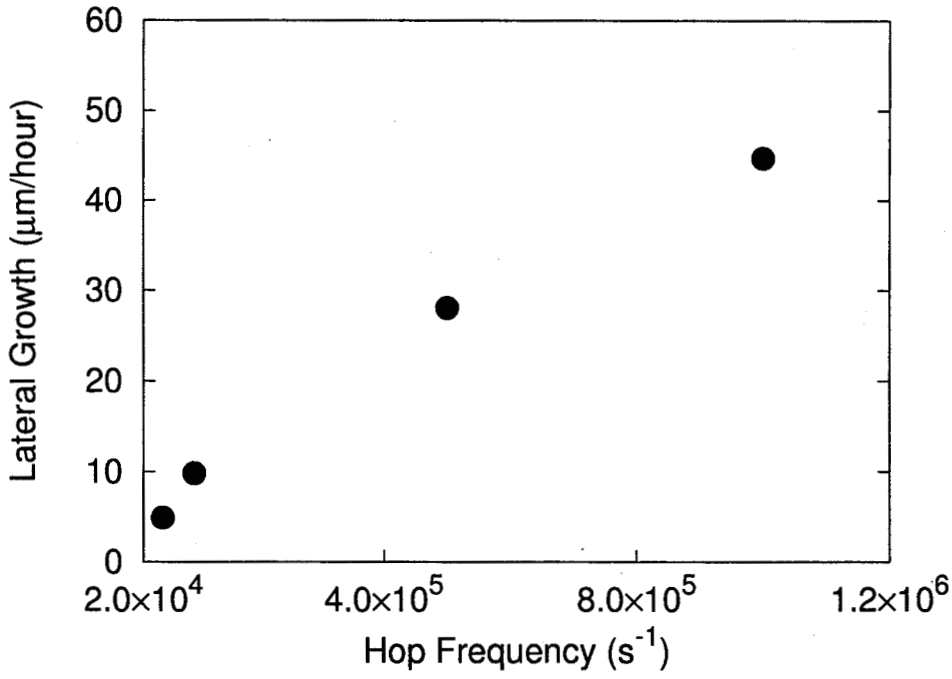

Fig. 7. Calculated lateral growth rates obtained from kinetic simulation.

well. The increase in group III adatom diffusion in the [110] direction is easily explained by the weaker bonding of the group III adatoms to Sb, as compared to either As or P. This would act to reduce the hop barrier for Ga adatoms (increasing hop frequency).

On the surface of InGaAs [20] and InGaNAs [21] Bi surfactant was found to smooth the surface, induce a (1×3) surface reconstruction, enhance the adatom diffusion length, and, at high concentrations, decrease the energy of surface steps. The Bi stabilized step edges were diffuse with many small islands nucleated adjacent to the step. The decrease in the Bi lateral growth rate at high Bi concentrations seen in fig. 6 might be explained by a similar transition in step structure. For the lower TMBi concentrations, Bi enhances lateral growth by reducing the hop barrier of Ga adatoms. At higher concentrations a second effect begins to dominate; Bi begins to reduce the step energy, which reduces the driving force for step propagation. With stabilized steps, the sticking coefficient would be low; thus, nucleation would be more likely and, as result, the lateral growth rate would decrease. A second hypothesis is that a buildup of Bi on the surface further modifies the surface structure in a manner that blocks Ga diffusion. This would, of course, also lead to a decreased step velocity. The former interpretation is favored, based on the observed surfactant effects of Bi in other systems.

6 Summary

TMSb and TMBi were used as surfactant precursors during OMVPE growth of GaAs on patterned substrates. Sb and Bi were both found to dramatically enhance GaAs (001) lateral growth anisotropy by increasing the [110] growth rate. Since Sb-Ga and Bi-Ga surface bonds are weaker than As-Ga bonds, the presence of these surfactants in the surface reconstruction is expected to reduce the hop barrier for diffusion of Ga adatoms. An increase in the frequency of [110] diffusion events reasonably accounts for the observed lateral growth enhancement observed for Sb and for Bi at low concentrations. Kinetic simulation supports the hypothesis that adatom hop frequency is the key parameter modified by these surfactants. Variation of this parameter leads to surface profiles similar to those observed experimentally. For high Bi concentrations, the [110] lateral growth rate begins to be reduced by the addition of more Bi. This is interpreted as due to a stabilization of the $[\bar{1}10]$ step edge with a consequent reduction in the adatom sticking coefficient.

Acknowledgements

The authors wish to thank the Department of Energy, Division of Basic Sciences, and Sandia National Laboratories for their support in funding the research presented in this article.

References

[1] H. Asai, J. Crystal Growth 80 (1987) 425.

[2] W. Reichert, R. Cohen, J. Crystal Growth 220 (2000) 364.

[3] W. Reichert, R. Cohen, J. Elect. Mat. 29 (1) (2000) 118.

[4] S.-I. Kim, M.-S. Kim, Y. Kim, S.-M. Hwang, B.-D. Min, C. S. Son, E. K. Kim, S.-K. Min, J. Crystal Growth 170 (1997) 665.

[5] A. Howard, L.W. Reith, D.C. Chapman, R.R. Wixom, G.B. Stringfellow, JAP (to be published).

[6] R. Lee, J. SHurtleff, C. Fetzer, G. B. Stringfellow, S. Lee, T. Seong, J. Appl. Phys. 87 (2000) 3730.

[7] R. Lee, C. Fetzer, S. Jun, D. Chapman, J. Shurtleff, G. Stringfellow, Y. Ok, T. Seong, J. Crystal Growth 233 (2001) 490.

[8] J. SHurtleff, R. Lee, C. Fetzer, G. Stringfellow, S. Lee, T. Seong, J. Crystal Growth 234 (2002) 327.

[9] S. Jun, G. Stringfellow, J. Shurtlef, R.-T. Lee, J. Crystal Growth 325 (2002) 15.

[10] T. Suzuki, T. Ichihashi, K. Kurihara, K. Nishi, J. Cryst. Growth 221 (2000) 31.

[11] R. Wixom, N. Modine, G. Stringfellow, Phys. Rev. B 64 (2001) 201332.

[12] R. Wixom, N. Modine, G. Stringfellow, Phys. Rev. B 67 (2003) 115309.

[13] L.Zhang, H. Tang, J. Schieke, M. Mavrikakis, T. Kuech, J. Appl. Phys. 92 (5) (2002) 2304.

[14] L. Zhang, H. T. adn T.F Kuech, Appl. Phys. Lett. 79 (19) (2001) 3059.

[15] C. Pei, B. Turk, J. Heroux, W. Wang, J. Vac. Sci. Technol. B 19 (4) (2001) 1426.

[16] K. Volz, V. Gambin, W. Ha, M. Wistey, H. Yuen, S.Bank, J. Harris, J. Crystal Growth 251 (2003) 360.

[17] A. Chakrabarti, K. Kunc, Phys. Rev. B 68 (2003) 045304.

[18] J. Shurtleff, S. Jun, G. Stringfellow, Appl. Phys. Lett. 78 (20) (2001) 3038.

[19] F. Dimroth, A. Howard, J. Shurtlef, G. Stringfellow, J. Appl. Phys. 91 (6) (2002) 3687.

[20] M.R. Pillai, S-S Kim, S.T. Ho, S.A. Barnett, J. Vac. Sci. Technol. B 18 (3) (2000) 1232.

[21] S. Tixier, M. Adamcyk, E.C. Young, J.H. Schmid, T. Tiedje, J. Crystal Growth 251 (2003) 449.

[22] K. Miki, D.R. Bowler, J.H.G Owen, G.A.D Briggs, K. Sakamoto, Phys. Rev. B 59 (1999) 14868

[23] B. Zvonkov, I. Karpovich, N. Baidus, D. Filatov, S. Morozov, Y. Y. Gushina, Nanotechnology 11 (2000) 221.

[24] G. Ehrlich, F.G. Hudda, J. Chem. Phys. 44 (1966) 1039.

[25] R.L. Schwoebel, J. Appl. Phys. 40 (1969) 614.

Theory of surfactant (Sb) induced reconstructions on InP(001)

R. R. Wixom
Department of Materials Science and Engineering, University of Utah, Salt Lake City, Utah 84112

N. A. Modine
Sandia National Laboratories, Albuquerque, New Mexico 87185

G. B. Stringfellow
College of Engineering, University of Utah, Salt Lake City, Utah 84112
(Received 31 July 2002; published 12 March 2003)

Surface structure is an important key to understanding surfactant mechanisms. Surface energies obtained via first principles can help determine the likely reconstructions of clean and surfactant covered surfaces. A general method for calculating accurate zero-temperature surface energies of arbitrarily complex material systems is discussed. Some common sources of error are systematically avoided. The resulting surface energies allow the construction of surface phase diagrams that illustrate surfactant induced changes to the surface. We have applied the described method to the Sb/InP(001) surface and created a surface phase diagram for this material. This diagram and our previously reported results for the GaP(001) surface are helpful in explaining bulk triple period ordering in GaInP and experimentally observed changes in surface structure.

DOI: 10.1103/PhysRevB.67.115309 PACS number(s): 68.35.Md, 81.10.Aj, 81.15.Aa, 81.15.Gh

I. INTRODUCTION

An understanding of surface mechanisms leads to improved control of epitaxial thin film properties. A knowledge of the growth surface, obtained through both experimental and theoretical means, has been helpful in exploring theories about morphological evolution, alloy composition, and ordering in a wide variety of materials systems. For example, investigation of GaInP (001) surface reconstructions has provided insight into the driving force for $CuPt_B$ ordering, which is induced by the P surface dimers.[1,2]

As a consequence of our improving knowledge of surface structure, surfactants are becoming an important tool for tailoring epitaxially grown semiconductor materials. Recently, Sb has been studied as a surfactant in organometallic vapor phase epitaxy (OMVPE) of GaInP. A small amount of Sb present during growth was found to reduce $CuPt_B$ ordering, while high concentrations of Sb induced triple period ordering in the solid.[3] Similar experiments revealed that Sb modified the surface structure,[1,4] enhanced dopant incorporation,[5,6] and induced a composition modulation.[7,8]

A principle mechanism by which surfactants effect epitaxial growth is modification of surface bonding. We have developed theoretical techniques to determine the energies of surfactant induced reconstructions and applied them to investigate Sb covered InP(001) surfaces, with the goal of explaining experimental observations. First we provide a detailed derivation of the technique and then discuss a specific application of the theory.

II. THEORY

The techniques we discuss in this paper have been applied to specific materials. However, they are developed for the general case and should readily transfer to other surfactants and materials systems.

There are a large number of possible reconstructions for a given surface and it is not possible to consider them all when trying to predict the most stable surface structure. However, a reasonable set of reconstructions can be chosen by considering experimental data, other similar materials, and the electron counting rule.[9] By comparing the surface energies of the chosen reconstructions, a likely structure for a given set of thermodynamic conditions can be predicted.

Surface energies can be calculated by using a slab model to simulate the surface of an epitaxial layer. One surface of a slab is reconstructed while the other surface is passivated by fictitious, fractionally charged, hydrogenlike atoms ($\frac{3}{4}$ charge when saturating group-V dangling bonds).[10] The total energy of the reconstructed slab can then be determined via Kohn-Sham density functional theory (DFT) calculations from which the surface free energy of the reconstruction is obtained.

Free energy is a function of partial pressures and temperature. Temperature affects surface energy directly through configurational and vibrational entropy and indirectly through modification of chemical potential. For most epitaxial systems, the indirect temperature effects are dominant. Therefore, it is useful to neglect the direct dependence on temperature and pressure and express the free energy as a function of the chemical potential, where dependence on temperature and partial pressures is implied. With this approximation, free energy Ω is then defined as

$$\Omega = E_{\text{total}} - \Sigma n_i \mu_i , \quad (1)$$

where E_{total} is the total energy and n_i and μ_i are the number and chemical potential of constituent i.

As long as the slab contains enough atomic layers to relax all surface induced strain, the free energy of a slab can be expressed as a sum of surface and bulk free energies

$$\Omega_{\text{slab}} = \sigma + N\Omega_{\text{bulk}}. \quad (2)$$

In this equation Ω_{slab} depends linearly on the number of bulk units N. The slope Ω_{bulk} is the bulk free energy per unit and the intercept is the total surface energy σ.

Using Eq. (1) to expand Eq. (2) and solving for σ provides

$$\sigma = E^{\text{slab}}_{\text{total}} - \Sigma n_i^{\text{slab}} \mu_i - N(E^{\text{bulk}}_{\text{total}} - \Sigma n_i^{\text{bulk}} \mu_i). \quad (3)$$

If we consider a system where the bulk consists of a binary material with a bulk unit containing one atom of each type, $n_i^{\text{bulk}} = 1$, and we can further reduce Eq. (3) to

$$\sigma = E^{\text{slab}}_{\text{total}} - \Sigma n_i^{\text{slab}} \mu_i - NE^{\text{bulk}}_{\text{total}} + N\Sigma \mu_i. \quad (4)$$

The total number of atoms of type i in the slab n_i^{slab} and a chosen value for N, can be used to define n_i^{surf}, the number of atoms of type i in the surface reconstruction using the relationship

$$n_i^{\text{surf}} = n_i^{\text{slab}} - N. \quad (5)$$

Now the total zero temperature surface energy can be written in a general form

$$\sigma = E^{\text{slab}}_{\text{total}} - NE^{\text{bulk}}_{\text{total}} - \Sigma n_i^{\text{surf}} \mu_i, \quad (6)$$

regardless of the number of bulk and surface species.

For a surface in equilibrium with bulk material $\Omega_{\text{bulk}} = 0$, a whole family of expressions for the surface energy σ can be generated by choosing different values of N. Note that all of these expressions give the same numerical value for σ. Common choices of N found in the literature, for III-V binaries, include $N = n_{\text{III}}^{\text{slab}}$, $N = n_{\text{V}}^{\text{slab}}$, and $N = \frac{1}{2}(n_{\text{III}}^{\text{slab}} + n_{\text{V}}^{\text{slab}})$. In principle, $N = 0$ is also a valid choice which would eliminate the need for calculating $E^{\text{bulk}}_{\text{total}}$. However, we will show that the bulk total energy $E^{\text{bulk}}_{\text{total}}$ can be calculated in a manner which is entirely consistent with the calculations of $E^{\text{slab}}_{\text{total}}$. On the other hand, the limits of the chemical potential are determined from calculations of the formation energy for the bulk elements which, due to the different crystal structures involved, cannot be done in a manner consistent with the calculations of $E^{\text{slab}}_{\text{total}}$. Therefore, it is preferred to chose a value of N that minimizes the coefficients of μ_i in the equation for the surface energy.

For a slab with one hydrogen terminated surface, the total surface energy σ contains the energy of the reconstructed surface σ_R as well as the energy of the hydrogen terminated surface σ_H. The energy contribution of the hydrogen termination will not affect the relative surface energies of the reconstructions. However, this nonphysical energy should be subtracted from the surface energy and can be calculated by applying the above approach to a slab where both surfaces are hydrogen terminated. Thus, the surface energy of a particular reconstruction R is given by $\sigma_R = \sigma - \sigma_H$.

The application of Eq. (6) appears straight forward, however the importance of the $NE^{\text{bulk}}_{\text{total}}$ term is probably overlooked by many. As pointed out by Boettger,[11] a separate calculation of the bulk energy introduces errors, associated with technical parameters such as plane-wave cutoff and

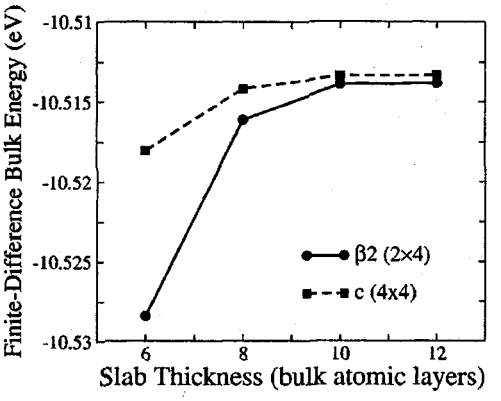

FIG. 1. GaP bulk energy calculated by finite-difference using the total energies of slabs with n and $n+\Delta n$ layers.

k-point sampling, which are magnified by the large factor N. To avoid these errors, it was proposed that $E^{\text{bulk}}_{\text{total}}$ be obtained from the difference in energy between two slabs of different thickness, or for some materials, a linear extrapolation of several such points.[12,13]

The total slab energy $E^{\text{slab}}_{\text{total}}$ only becomes a linear function of N when the slab is thick enough to relax all surface induced strain. Using the data from a set of increasingly thick slabs with the same reconstruction, we apply a finite-difference method

$$E^{\text{bulk}}_{\text{total}}(N) = \frac{E^{\text{slab}}_{\text{total}}(N+\Delta N) - E^{\text{slab}}_{\text{total}}(N)}{\Delta N}, \quad (7)$$

for calculating the bulk energy. As the slab thickness increases, the finite-difference bulk energies converge. Figure 1 illustrates that as many as 10 atomic layers can be needed to converge $E^{\text{bulk}}_{\text{total}}$ for the GaP(001) $\beta 2(2\times4)$ reconstruction. On the other hand, a $c(4\times4)$ reconstructed slab requires only eight bulk layers to reach the linear regime. Once each of the slabs converges to a linear dependence on N, we obtain $E^{\text{bulk}}_{\text{total}} = -10.514$ eV, regardless of structure or surface stoichiometry. This indicates that our calculations are well converged with respect to technical parameters.

Since all of the slabs converge at a different rate, the error in the bulk energy will not simply cancel when slabs of the same thickness with different reconstructions are compared, and the discrepancy will be exacerbated when thinner slabs are used. Consider the two reconstructed slabs in Fig. 1. There is a 0.01 eV discrepancy in the bulk energy derived from $c(4\times4)$ and $\beta 2(2\times4)$ slabs of six atomic layers. If these slabs were used to calculate surface energies, the discrepancy would be magnified by the number of bulk units. A comparison of the surface energies would then include a 0.3 eV error, which is certainly large enough to be of concern. If slabs of 12 atomic layers were used instead, the discrepancy in the bulk energy is only 0.5 meV and the resulting error in surface energy would be 0.023 eV. In order for a meaningful and confident comparison to be made, each slab must be thick enough to ensure that $E^{\text{bulk}}_{\text{total}}$ has converged and is consistent with the values obtained for the other reconstructions.

Equilibrium with bulk material requires that $\Sigma n_i^{\text{bulk}} \mu_i = E_{\text{total}}^{\text{bulk}}$; thus, for a reconstruction on a binary III-V material, such as GaAs, the surface energy is a function of only one independent variable. We take this to be the group-V chemical potential, which corresponds to the choice $N = n_{\text{III}}^{\text{slab}}$. If another atom type is added to the reconstruction, as in the case of a surfactant covered surface, the surface energy becomes a function of two variables, with the second variable being $\mu_{\text{surfactant}}$.

In equilibrium, a reconstruction can only appear on the surface if it has the lowest surface energy σ_R for some set of chemical potentials μ_i. For each chemical potential, an allowable range is defined by the growth of elemental bulk material.[14] Thus, for III-V surfaces, the chemical potential of group-V species has upper and lower bounds defined by

$$\mu_V(\text{bulk}) - \Delta H_f^{\text{III-V}} \leq \mu_V \leq \mu_V(\text{bulk}), \tag{8}$$

where $\Delta H_f^{\text{III-V}}$ is the enthalpy of formation for the bulk III-V unit.

For a surfactant such as Sb, the upper bound of the chemical potential will also be determined by the growth of bulk material. However, since a typical surfactant is not significantly incorporated into the growing epitaxial layer, $\mu_{\text{surfactant}}$ and μ_{III} can essentially vary independently. Therefore, growth of bulk Ga does not set a minimum on $\mu_{\text{surfactant}}$, which can be arbitrarily negative. In practice, increasingly negative values of $\mu_{\text{surfactant}}$ are only interesting until the surfactant is removed from the system completely, and the clean III-V(001) surface is stabilized. Using Eq. (6) and the boundaries defined by Eq. (8), a surface phase diagram can be constructed.

III. COMPUTATIONAL METHODS

A supercell containing a reconstructed slab was created for each considered surface structure. The Vienna *Ab Initio* Simulation Package (VASP) electronic structure code was used to calculate total energies and forces within the local density approximation.[15] Ultrasoft Vanderbilt pseudopotentials were obtained from the VASP pseudopotential database.[16,17]

The bottom III-V bilayer and the terminating hydrogens were held fixed, while all other atoms were allowed to relax until atomic forces were less than 0.01 eV/Å. Bulk energies were obtained from Eq. (7) using two sufficiently thick slabs. Slabs were considered sufficiently thick when $E_{\text{total}}^{\text{bulk}}(N)$ was converged within 0.5 meV, which for this work required slabs with 8 to 14 bulk atomic layers.

Sufficient vacuum space was included in each supercell to avoid interaction between the slab and its periodic image above and below. We calculated the energy of a slab several times with increasing vacuum space and determined that beyond 6 Å, the amount of vacuum space has negligible effect on the total energy of the slab. For our calculations, at least 10 Å of vacuum was used to separate a slab from its periodic image.

Convergence of total energies with respect to k-point sampling and plane-wave cutoff was investigated. k-point sampling equivalent to at least 64 k-points within the (1×1) surface Brillouin zone and a plane-wave cutoff of 12.5 Ry were used for all surface calculations. Using these parameters, the bulk InP lattice constant was determined to be 5.828 Å, which was used to fix the in-plane lattice constant of the slab.

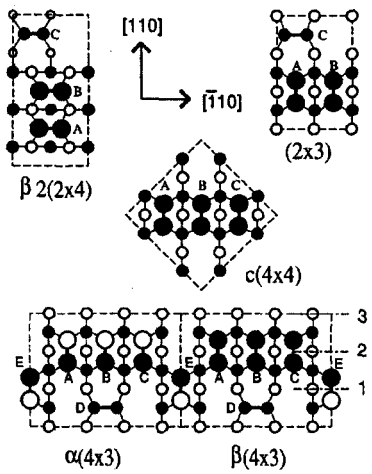

FIG. 2. Surface reconstructions considered (top views). Open (closed) circles represent group III (group V) atoms. Larger circles represent the top layer.

IV. APPLICATION AND RESULTS

The methods described above were applied to the Sb covered InP(001) surface. The surface reconstructions shown in Fig. 2 were investigated for the stoichiometric variations listed in Table I. For typical OMVPE growth parameters the

TABLE I. Stoichiometry of the structures investigated. "A–E" indicate the group V atoms for the dimer positions shown in Fig. 2. "2nd layer" indicates all the atoms in the first buried layer of the double layer reconstructions.

Structure	A	B	C	D	E	2nd layer
$\beta2(2\times4)-1$	P	P	P			
$\beta2(2\times4)-2$	Sb	Sb	Sb			
$\beta2(2\times4)-3$	Sb	Sb	P			
$\beta2(2\times4)-4$	Sb	P	P			
$(2\times3)-1$	Sb	Sb	Sb			P
$(2\times3)-2$	Sb	Sb	Sb			Sb
$c(4\times4)-1$	P	P	P			P
$c(4\times4)-2$	Sb	Sb	Sb			P
$c(4\times4)-3$	Sb	Sb	Sb			Sb
$\alpha(4\times3)-1$	P	P	P	P	P	P
$\alpha(4\times3)-2$	Sb	Sb	Sb	Sb	Sb	P
$\alpha(4\times3)-3$	Sb	Sb	Sb	Sb	Sb	Sb
$\beta(4\times3)-1$	P	P	P	P	P	P
$\beta(4\times3)-2$	P	P	P	Sb	Sb	Sb
$\beta(4\times3)-3$	Sb	Sb	Sb	P	P	P
$\beta(4\times3)-4$	Sb	Sb	Sb	Sb	P	Sb
$\beta(4\times3)-5$	Sb	Sb	Sb	Sb	Sb	Sb

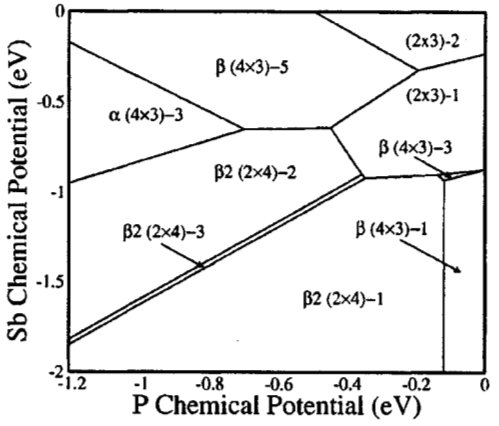

FIG. 3. Phase diagram for Sb/InP(001) surface. The stoichiometry of each stable phase is given in Table I. Chemical potentials are relative to bulk P and Sb so that $\mu_P = \mu - \mu_P^{bulk}$ and $\mu_{Sb} = \mu - \mu_{Sb}^{bulk}$.

group III elements are depleted at the surface,[18] suggesting that only anion rich reconstructions need to be considered.

The most stable of the considered reconstructions was found for the allowable values of μ_P and μ_{Sb} and this information is presented in Fig. 3. Similar results for Sb covered GaP(001) have been previously reported.[19]

A minimum value of μ_{Sb} in the Sb/InP(001) surface phase diagrams corresponds to a P terminated surface. Our calculations predict that this P-terminated InP surface is $\beta 2(2\times4)$ for most values of μ_P, but will transition to $\beta(4\times3)$ for extremely high values of μ_P. As Sb is added to the $\beta 2(2\times4)$ surface, the structure is retained; Sb substitutes for P atoms without changing the reconstruction. For high values of μ_{Sb} and μ_P the structure changes significantly and double layer P and Sb reconstructions become stable. Surprisingly, (2×3) structures are predicted to be stable although they violate Pashley's electron counting rule.[9]

The presence of $(\times3)$ surface structures in the high μ_{Sb} limit may explain the recent observance of triple period ordering in GaInP grown by OMVPE,[3] and the change in surface structure detected by surface photoabsorption (SPA).[4] Previous calculations indicate that $(\times3)$ surface structures provide a thermodynamic driving force for triple period ordering.[19]

V. CONCLUSIONS

In summary, a general method for calculating surface energy was developed and applied to a relevant materials science problem. Following the prescribed method, density functional theory and the local density approximation were used to calculate total energies for several possible Sb covered InP(001) surfaces. Surface energies were determined and used to construct a surface phase diagram, which is useful in developing theories to explain experimentally observed phenomena. Identification of surface reconstruction is a critical step toward investigation of growth processes such as adatom diffusion, step edge attachment, island nucleation, and morphological and compositional evolution.

ACKNOWLEDGMENTS

Sandia is a multiprogram laboratory operated by Sandia Corporation, a Lockheed Martin Company, for the United States Department of Energy under Contract No. DE-AC04-94AL85000. This work was partially supported by the Division of Materials Science and Engineering, Office of Basic Energy Sciences, U.S. DOE. Work at the University of Utah was supported by the Department of Energy under Contract No. DE-FG03-93ER45485.

[1] G. B. Stringfellow, J. K. Shurtleff, R. T. Lee, C. M. Fetzer, and S. W. Jun, J. Cryst. Growth **221**, 1 (2000).
[2] S. Froyen and A. Zunger, Phys. Rev. Lett. **66**, 2132 (1991).
[3] C. M. Fetzer, R. T. Lee, J. K. Shurtleff, G. B. Stringfellow, S. Lee, and T. Y. Seong, Appl. Phys. Lett. **76**, 1440 (2000).
[4] R. T. Lee, J. K. Shurtleff, C. M. Fetzer, G. B. Stringfellow, S. Lee, and T. Y. Seong, J. Appl. Phys. **87**, 3730 (2000).
[5] F. Dimroth, A. Howard, J. K. Shurtleff, and G. B. Stringfellow, J. Appl. Phys. **91**, 3687 (2002).
[6] J. K. Shurtleff, S. W. Jun, and G. B. Stringfellow, Appl. Phys. Lett. **78**, 3038 (2001).
[7] C. M. Fetzer, R. T. Lee, J. K. Shurtleff, G. B. Stringfellow, S. Lee, and T. Y. Seong, Appl. Phys. Lett. **78**, 1376 (2001).
[8] J. K. Shurtleff, R. T. Lee, C. M. Fetzer, and G. B. Stringfellow, Appl. Phys. Lett. **75**, 1914 (1999).
[9] M. D. Pashley, Phys. Rev. B **40**, 10 481 (1989).
[10] K. Shiraishi, J. Phys. Soc. Jpn. **59**, 3455 (1990).
[11] J. C. Boettger, Phys. Rev. B **49**, 16 798 (1994).
[12] V. Fiorentini and M. Methfessel, J. Phys.: Condens. Matter **8**, 6525 (1996).
[13] N. A. Modine and E. Kaxiras, Mater. Sci. Eng., B **67**, 1 (1999).
[14] Guo-Xin Qian, R. M. Martin, and D. J. Chadi, Phys. Rev. B **38**, 7649 (1988); Phys. Rev. Lett. **60**, 1962 (1988).
[15] G. Kresse and J. Hafner, Phys. Rev. B **47**, 558 (1993); **49**, 14 251 (1994); G. Kresse and J. Furthmuller, *ibid.* **54**, 11 169 (1996); Comput. Mater. Sci. **6**, 15 (1996).
[16] D. Vanderbilt, Phys. Rev. B **41**, 7892 (1990).
[17] G. Kresse and J. Hafner, J. Phys.: Condens. Matter **6**, 8245 (1994).
[18] Gerald B. Stringfellow, *Organometallic Vapor-Phase Epitaxy: Theory and Practice* (Academic Press, San Diego, 1999).
[19] R. R. Wixom, G. B. Stringfellow, and N. A. Modine, Phys. Rev. B **64**, 201322 (2001).

PHYSICAL REVIEW B, VOLUME 64, 201322(R)

Theory of Sb-induced triple-period ordering in GaInP

R. R. Wixom and G. B. Stringfellow
Department of Materials Science and Engineering, University of Utah, Salt Lake City, Utah 84112

N. A. Modine
Sandia National Laboratories, Albuquerque, New Mexico 87185

(Received 27 July 2001; published 5 November 2001)

During organo-metallic vapor phase epitaxy (OMVPE) of GaInP (001) layers, the structure of the growth surface has a profound influence on the microstructure, and the optical and electrical properties of the resulting bulk material. The $\beta2(2\times4)$ surface, terminated with P dimers, provides a thermodynamic driving force for $CuPt_B$ ordering. Recently, surfactants such as Sb have been used to reduce this driving force. The use of surfactants to control the surface structure during growth has allowed for band-gap tailoring and the fabrication of heterostructures with no change in solid composition across the interface. Another exciting discovery was that high coverages of Sb induced a bulk triple period ordering. To further our understanding of these phenomena, the P terminated GaP(001) surface was studied via first principles calculations based on the Kohn-Sham density functional theory within the local density approximation (LDA). It was determined that under increasingly P-rich conditions, the $\beta2(2\times4)$ and then the $c(4\times4)$ reconstructions are stable. When the surface is covered with Sb, several different reconstructions are found to be stable in the allowable range of chemical potentials. Under lower group-V coverages the $\beta2(2\times4)$ is stable, while at high Sb coverage, (4×3) and (2×3) reconstructions are stable. We propose that these $(\times3)$ reconstructions explain the triple period ordering seen in GaInP grown with Sb as a surfactant. Total-energy calculations confirm that $(\times3)$ reconstructions provide a thermodynamic driving force for A-variant triple period ordering.

DOI: 10.1103/PhysRevB.64.201322 PACS number(s): 68.35.Md, 31.15.Ar, 68.43.Bc, 81.10.Aj

I. INTRODUCTION

Several recent experimental studies have used Sb as a surfactant on III-V semiconductor surfaces. These studies have shown Sb to exhibit amazing surfactant effects that are both scientifically interesting and potentially useful for technological applications. Sb has been used as a surfactant in the epitaxial growth of GaInP to control ordering and induce lateral compositional modulations.[1–5] In GaAs, Sb has been shown to change dopant incorporation.[6] The surface structure, as well as the electronic and optical properties of these materials, are modified by the addition of Sb during growth, but the actual mechanisms have yet to be explained.

The GaInP(001) growth surface has not been studied as extensively as the GaAs(001) surface. However, the few studies that have been done[7–9] seem to agree that GaInP reconstructs similarly to GaAs.[10,11] Under the conditions of organo-metallic vapor phase epitaxy (OMVPE), these reconstructions consist of $[\bar{1}10]$ P dimers, which have a much shorter bond length than the bulk interatomic distance. These dimers create a periodic array of compressive and tensile strain that is thought to be the driving force for the B-variants of CuPt ordering.[12] The term B-variant designates CuPt ordering in the $[\bar{1}10]$ direction, while A-variant ordering is along the [110] direction.

When the surface is covered with Sb, which has a dimer bond length greater than the P dimer bond length, the $[\bar{1}10]$ P dimers are replaced with $[\bar{1}10]$ Sb dimers and the driving force for $CuPt_B$ ordering is reduced.[13] Since the band gap of GaInP is strongly dependent on the degree of order, researchers have modulated the band gap by as much as 135 meV using Sb as a surfactant.[2] This phenomenon provides a simple means to fabricate heterostructure devices with no change in the solid composition across the interface.

With increasing Sb flux onto the surface, an A-variant triple period ordering (TPO) is observed.[3] The surface photoabsorption peaks characteristic of $[\bar{1}10]$ surface dimers are absent from the spectra indicating a significant change in surface structure.[1,13] A $(\times3)$ periodic double layer Sb surface reconstruction would produce a triple period [110] modulated strain field, which is consistent with A-variant TPO. It has been proposed that A-variant TPO results from a (2×3) surface structure,[3,5] but until now, theory has not shown this reconstruction to be stable for any Sb-terminated surface. Experiment and theory have shown that several (4×3) structures are stable on [001] III-Sb surfaces,[14,15] and recently, Nosho *et al.* used scanning tunneling microscopy to image $\beta(4\times3)$ and (2×3)-like structures on Sb covered InAs (001) surfaces.[16]

Previous theoretical studies of the P-rich GaInP surface have shown that the reconstructions are largely independent of the group-III composition.[7] For both GaP and InP, this surface undergoes a $\beta2(2\times4)$ to $c(4\times4)$ surface phase transition under increasing group-V chemical potential.[7,8] Considering GaP and InP separately avoids the pitfalls of the virtual crystal approximation and the difficulty of representing a partially ordered pseudobinary material under the constraints of periodic boundary conditions. For these reasons, this study considers Sb-covered GaP(001) surfaces instead of attempting to model the pseudobinary system. Additional information about the effects of surface reconstruction on ordering in the alloy is then obtained by calculating and comparing total energies of slabs with indium atoms substituted into the first bulk Ga layer.

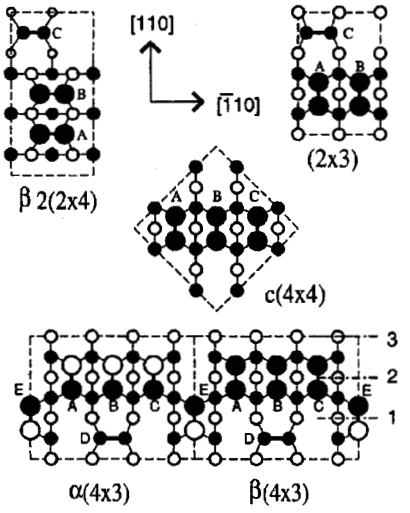

FIG. 1. Surface reconstructions considered (top views). Open (closed) circles represent Ga (group-V—either P or Sb) atoms. Larger circles represent the top layer.

II. COMPUTATIONAL METHODS

We have compared the stability of the reconstructions previously shown to be stable on V-terminated GaInP and III-Sb (001) surfaces, as well as the (2×3) structure. The structures considered in this study are shown in Fig. 1. The surface energies of these structures, obtained via Kohn-Sham density functional theory (DFT) calculations, were used to determine the relative stability.

In order to represent a surface, we used a slab model with the desired reconstruction on one surface and fictitious hydrogenlike atoms with the appropriate charge (3/4 when saturating P dangling bonds) to terminate the other surface.[17] The bottom bilayer of GaP and the hydrogens were held fixed, while all other atoms were allowed to relax until atomic forces were less than 0.01 eV/Å. At least 10 Å of vacuum was used to separate a slab from its periodic image.

The Vienna *ab-initio* simulation package (VASP) electronic structure code was used to calculate total energies and forces within the local density approximation.[18] Ultrasoft Vanderbilt pseudopotentials were obtained from the VASP pseudopotential database.[19,20] Convergence of these energies with respect to k-point sampling and plane-wave cutoff was investigated. K-point sampling equivalent to at least 64 k-points within the (1×1) surface Brillouin zone and a plane-wave cutoff of 12.5 Ry were used for all surface calculations. Using these parameters, the bulk GaP lattice constant was determined to be 5.401 Å, and the in-plane lattice constant of the slabs was fixed at this value.

We calculated surface energies by extrapolating the total energies of several increasingly thick slabs to zero thickness, as originally proposed by Boettger[21] and Fiorentini and Methfessel.[22] Modine and Kaxiras generalized this method to account for the stoichiometry of compound semiconductors,[23] and we further generalized their method for multicomponent systems. For a sufficiently thick slab, the surface energy σ is given by the equation,

$$\Omega_{slab}=\sigma+N\Omega_{bulk}, \tag{1}$$

where Ω represents the zero-temperature grand-canonical free energy. Since Ω_{slab} is a linear function of the number of bulk units N, linear extrapolation to zero slab thickness gives the surface energy. In our case, the surface energy σ contains the energy of the reconstructed surface σ_R as well as the energy of the hydrogen terminated surface σ_H. For our extrapolations, slabs thick enough to ensure a linear dependence on N were used. Sufficient slab thickness was found to be somewhat different for each reconstruction, depending on how far the surface strain penetrated into the slab, but was typically 3 to 5 bulklike GaP bilayers.

Substituting the definition of Ω for a given reconstruction R into Eq. (1), we obtain

$$\sigma_R=E^R_{N\to0}-\sigma_H-\Delta n^R_P\mu_P-\Delta n^R_{Sb}\mu_{Sb}-\Delta n^R_H\mu_H, \tag{2}$$

where $E^R_{N\to0}$ is the result of extrapolating the total energies of a series of slabs to zero thickness. The Δn and μ terms are the number of excess (nonstoichiometric) atoms and the chemical potential for each type of atom. Applying the same formalism to slabs (denoted by an H superscript) with both surfaces terminated by hydrogen gives

$$2\sigma_H=E^H_{N\to0}-\Delta n^H_P\mu_P-\Delta n^H_H\mu_H. \tag{3}$$

Since the hydrogen-terminated slabs are chosen such that $2\Delta n^R_H=\Delta n^H_H$, the μ_H terms cancel leaving two independent variables (μ_P and μ_{Sb}) in σ_R.

A given reconstruction will only appear on the Sb/GaP(001) surface if it has the lowest surface energy σ for some μ_P and μ_{Sb} within an allowable range of chemical potentials.[24] For III-V surfaces that are in equilibrium with bulk III-V material, μ_{III} and μ_V are related, and for each chemical potential, an allowable range is defined by the growth of bulk III and bulk V material.[25] Thus, the chemical potential of P has upper and lower bounds defined by

$$\mu_P(bulk)-\Delta H^{GaP}_f\leq\mu_P\leq\mu_P(bulk). \tag{4}$$

For a surfactant such as Sb, the upper bound of the chemical potential will also be determined by the growth of bulk material. However, since Sb is not significantly incorporated into the growing epitaxial layer, μ_{Sb} and μ_{Ga} can vary independently. Therefore, growth of bulk Ga does not set a minimum on μ_{Sb}, which can be arbitrarily negative. In practice, increasingly negative values of μ_{Sb} are only interesting until Sb is removed from the system completely, and the clean GaP(001) surface is stabilized.

The basic surface reconstructions shown in Fig. 1 were investigated for the stoichiometric variations listed in Table I. Because the method of calculation makes the approximation of 0 K, each stoichiometric change was treated as a separate phase even if the structure was otherwise the same. However, at higher temperatures, stoichiometric changes may not be abrupt, and in experiments, it is possible to have a mixture of phases on the surface, making it difficult to distinguish similar structures.[16]

TABLE I. Stoichiometry of the structures investigated. "A-E" indicate the group V atoms for the dimer positions shown in Fig. 1. "2nd layer" indicates all the atoms in the first buried layer of the double-layer reconstructions.

Structure	A	B	C	D	E	2nd layer
$\beta2(2\times4)-1$	P	P	P	–	–	–
$\beta2(2\times4)-2$	Sb	Sb	Sb	–	–	–
$\beta2(2\times4)-3$	Sb	Sb	P	–	–	–
$\beta2(2\times4)-4$	Sb	P	P	–	–	–
$(2\times3)-1$	Sb	Sb	Sb	–	–	P
$(2\times3)-2$	Sb	Sb	Sb	–	–	Sb
$c(4\times4)-1$	P	P	P	–	–	P
$c(4\times4)-2$	Sb	Sb	Sb	–	–	P
$c(4\times4)-3$	Sb	Sb	Sb	–	–	Sb
$\alpha(4\times3)-1$	P	P	P	P	P	P
$\alpha(4\times3)-2$	Sb	Sb	Sb	Sb	Sb	P
$\alpha(4\times3)-3$	Sb	Sb	Sb	Sb	Sb	Sb
$\beta(4\times3)-1$	P	P	P	P	P	P
$\beta(4\times3)-2$	P	P	P	Sb	Sb	Sb
$\beta(4\times3)-3$	Sb	Sb	Sb	P	P	P
$\beta(4\times3)-4$	Sb	Sb	Sb	Sb	P	Sb
$\beta(4\times3)-5$	Sb	Sb	Sb	Sb	Sb	Sb

III. RESULTS

From the preliminary bulk calculation, the enthalpy of formation for GaP was calculated to be 1.34 eV. For the clean P-terminated GaP(001) surface, we found the $\beta2(2\times4)$ and then the $c(4\times4)$ structures to be stable under increasing P chemical potential. These results are in excellent agreement with previous work.[7,8]

The surface phase diagram for the Sb-covered GaP(001) surface is shown in Fig. 2. The most exciting features are the $\beta(4\times3)$ and (2×3) structures which are stable for high values of μ_{Sb} within the allowable range of chemical potentials. It is somewhat surprising that the (2×3) structure, which does not satisfy the electron counting rule,[26] is stable. The $\alpha(4\times3)$ and $\beta(4\times3)$ reconstructions have a similar structure with different stoichiometry, but the $\alpha(4\times3)$ reconstruction is not stable on the Sb/GaP(001) surface. The $\beta(4\times3)$ and (2×3) structures differ only by a shifted dimer and the substitution of a Ga atom for a group-V atom. We believe that the $\beta(4\times3)$ and (2×3) surface reconstructions explain the appearance of A-variant TPO in GaInP under high Sb chemical potential.[3] The Sb dimers in the top layer of these reconstructions compress the Ga row directly under the dimer bonds (labeled as 2 in Fig. 1) and create a tensile

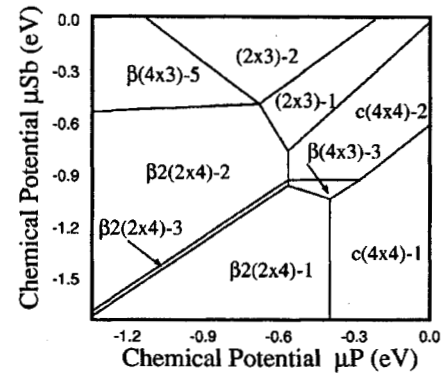

FIG. 2. Phase diagram for Sb/GaP(001) surface. The stoichiometry of each stable phase is given in Table I. Chemical potentials are relative to bulk P and Sb so that $\mu_P=\mu-\mu_P^{bulk}$ and $\mu_{Sb}=\mu-\mu_{Sb}^{bulk}$.

strain in the Ga rows on either side of the dimers (labeled as rows 1 and 3). In the alloy GaInP, the larger indium atoms will prefer to occupy rows 1 and 3, while the smaller Ga atoms will reside in row 2, resulting in triple period ordering.[5] Since this theory suggests that the Sb dimers induce ordering in the [110] direction, it is consistent with A-variant[27] TPO.

Once stability of the $\beta(4\times3)$ and (2×3) structures was established, the thermodynamic driving force for TPO was investigated by substituting indium atoms into the first buried Ga layer of the $\beta(4\times3)$ structure. In this layer, we considered three distinct rows of atoms which are labeled in Fig. 1. Indium atoms were substituted for the Ga atoms in each row and total energies were calculated. The configuration with indium atoms in row 1 (row 3) are 400 meV (200 meV) lower in energy than with indium substituted into row 2. These results support the simple theory of surface-induced ordering described above and show that it properly captures the physics of this system.

IV. SUMMARY AND CONCLUSION

Ab initio LDA calculations were used to determine stable reconstructions for the Sb-covered GaP(001) surface. The $\beta(4\times3)$ and (2×3) reconstructions are stable within the allowed range of chemical potentials, and provide a theoretical explanation for triple period ordering in GaInP. Total-energy calculations show that the $\beta(4\times3)$ structure produces a thermodynamic driving force for A-variant triple period ordering. This study adds to a growing collection of evidence indicating that bulk ordering in pseudobinary III-V materials is strongly influenced by surface reconstruction.

[1] R.T. Lee, J.K. Shurtleff, C.M. Fetzer, G.B. Stringfellow, S. Lee, and T.Y. Seong, J. Appl. Phys. **87**, 3730 (2000).

[2] J.K. Shurtleff, R.T. Lee, C.M. Fetzer, and G.B. Stringfellow, Appl. Phys. Lett. **75**, 1914 (1999).

[3] C.M. Fetzer, R.T. Lee, J.K. Shurtleff, G.B. Stringfellow, S. Lee, and T.Y. Seong, Appl. Phys. Lett. **76**, 1440 (2000).

[4] C.M. Fetzer, R.T. Lee, J.K. Shurtleff, G.B. Stringfellow, S. Lee, and T.Y. Seong, Appl. Phys. Lett. **78**, 1376 (2001).

[5] T. Suzuki, T. Ichihashi, K. Kurihara, and K. Nishi, J. Cryst. Growth **221**, 31 (2000).

[6] J.K. Shurtleff, S.W. Jun, and G.B. Stringfellow, Appl. Phys. Lett. **78**, 3038 (2001).

[7] S. Froyen and A. Zunger, Phys. Rev. B **53**, 4570 (1996).

[8] N. Esser, W.G. Schmidt, J. Bernhoic, A.M. Frisch, P. Vogt, M. Zorn, M. Pristovsek, W. Richter, F. Bechstedt, Th. Hannappel, and S. Visbeck, J. Vac. Sci. Technol. B **17**, 1691 (1999).

[9] P. Vogt, K. Ludge, M. Zorn, M. Pristovsek, W. Braun, W. Richter, and N. Esser, J. Vac. Sci. Technol. B **18**, 2210 (2000).

[10] K. Shiraishi, T. Ito, Y.Y. Suzuki, H. Kageshima, K. Kanisawa, and H. Yamaguchi, Surf. Sci. **433-435**, 382 (1999).

[11] J.E. Northrop and S. Froyen, Phys. Rev. B **50**, 2015 (1994).

[12] S. Froyen and A. Zunger, Phys. Rev. Lett. **66**, 2132 (1991).

[13] G.B. Stringfellow, J.K. Shurtleff, R.T. Lee, C.M. Fetzer, and S.W. Jun, J. Cryst. Growth **221**, 1 (2000).

[14] W. Barvosa-Carter, A.S. Bracker, J.C. Culbertson, B.Z. Nosho, B.V. Shanabrook, L.J. Whitman, Hanchul Kim, N.A. Modine, and E. Kaxiras, Phys. Rev. Lett. **84**, 4649 (2000).

[15] N.A. Modine, Hanchul Kim, and E. Kaxiras, in *Morphological and Compositional Evolution of Heteroepitaxial Semiconductor Thin Films*, edited by J. Mirecki Millunchick, A. L. Barabasi, N. A. Modine and E. D. Jones, MRS Symposium Proceedings No. **618** (Materials Research Society, Pittsburgh, 2000), p. 11.

[16] B.Z. Nosho, B.V. Shanabrook, B.R. Bennet, W. Barvosa-Carter, W.H. Weinberg, and L.J. Whitman, Surf. Sci. **478**, 1 (2001).

[17] K. Shiraishi, J. Phys. Soc. Jpn. **59**, 3455 (1990).

[18] G. Kresse and J. Hafner, Phys. Rev. B **47**, 558 (1993); **49**, 14 251 (1994); G. Kresse and J. Furthmuller, *ibid.* **54**, 11 169 (1996); Comput. Mater. Sci. **6**, 15 (1996).

[19] D. Vanderbilt, Phys. Rev. B **41**, 7892 (1990).

[20] G. Kresse and J. Hafner, J. Phys.: Condens. Matter **6**, 8245 (1994).

[21] J.C. Boettger, Phys. Rev. B **49**, 16 798 (1994).

[22] V. Fiorentini and M. Methfessel, J. Phys.: Condens. Matter **8**, 6525 (1996).

[23] N.A. Modine and E. Kaxiras, Mater. Sci. Eng., B **67**, 1 (1999).

[24] E. Kaxiras, K.C. Pandey, Y. Bar-Yam, and J.D. Joannopoulos, Phys. Rev. Lett. **56**, 2819 (1986); E. Kaxiras, Y. Bar-yam, J.D. Joannopoulos, and K.C. Pandey, *ibid.* **57**, 106 (1986); Phys. Rev. B **35**, 9625 (1987); **35**, 9636 (1987).

[25] Guo-Xin Qian, R.M. Martin, and D.J. Chadi, Phys. Rev. B **38**, 7649 (1988); Phys. Rev. Lett. **60**, 1962 (1988).

[26] M.D. Pashley, Phys. Rev. B **40**, 10 481 (1989).

[27] For A-variant (B-variant) ordering the direction of order is in the [110] ([$\bar{1}$10]) direction.

Distribution

No.	Mail Stop	Organization	Name
1	MS. 0841	9100	Tom Bickel
1	MS 323	1011	Donna Chavez
2	MS 0899	9616	Technical Library
1	MS 9018	8945-1	Central Technical Files